Optical Coherence Tomography Minimum Intensity as an Objective Measure for the Detection of Hydroxychloroquine Toxicity

Ali M. Allahdina,[1] Paul F. Stetson,[2] Susan Vitale,[1] Wai T. Wong,[1] Emily Y. Chew,[1] Fredrick L. Ferris III,[1] Paul A. Sieving,[1] and Catherine Cukras[1]

[1]National Eye Institute, National Institutes of Health, Bethesda, Maryland, United States
[2]Research and Development, Carl Zeiss Meditec, Inc., Dublin, California, United States

Correspondence: Catherine Cukras, Division of Epidemiology and Clinical Research and Ophthalmic Genetics and Visual Function Branch, National Eye Institute, National Institute of Health, Bethesda, MD 20892, USA; cukrasc@nei.nih.gov.

Submitted: July 20, 2017
Accepted: March 6, 2018

Citation: Allahdina AM, Stetson PF, Vitale S, et al. Optical coherence tomography minimum intensity as an objective measure for the detection of hydroxychloroquine toxicity. *Invest Ophthalmol Vis Sci*. 2018;59:1953–1963. https://doi.org/10.1167/iovs.17-22668

Purpose. As optical coherence tomography (OCT) minimum intensity (MI) analysis provides a quantitative assessment of changes in the outer nuclear layer (ONL), we evaluated the ability of OCT-MI analysis to detect hydroxychloroquine toxicity.

Methods. Fifty-seven predominantly female participants (91.2% female; mean age, 55.7 ± 10.4 years; mean time on hydroxychloroquine, 15.0 ± 7.5 years) were enrolled in a case-control study and categorized into affected (i.e., with toxicity, $n = 19$) and unaffected ($n = 38$) groups using objective multifocal electroretinographic (mfERG) criteria. Spectral-domain OCT scans of the macula were analyzed and OCT-MI values quantitated for each subfield of the Early Treatment Diabetic Retinopathy Study (ETDRS) grid. A two-sample U-test and a cross-validation approach were used to assess the sensitivity and specificity of toxicity detection according to OCT-MI criteria.

Results. The medians of the OCT-MI values in all nine of the ETDRS subfields were significantly elevated in the affected group relative to the unaffected group ($P < 0.005$ for all comparisons), with the largest difference found for the inner inferior subfield ($P < 0.0001$). The receiver operating characteristic analysis of median MI values of the inner inferior subfields showed high sensitivity and high specificity in the detection of toxicity with area under the curve = 0.99.

Conclusions. Retinal changes secondary to hydroxychloroquine toxicity result in increased OCT reflectivity in the ONL that can be detected and quantitated using OCT-MI analysis. Analysis of OCT-MI values demonstrates high sensitivity and specificity for detecting the presence of hydroxychloroquine toxicity in this cohort and may contribute additionally to current screening practices.

Keywords: optical coherence tomography, hydroxychloroquine, retina toxicity

Hydroxychloroquine is used widely in rheumatology, treating a host of autoimmune diseases, including systemic lupus erythematosus, rheumatoid arthritis, and Sjögren's syndrome.[1] Although hydroxychloroquine is generally well tolerated by patients, the main limit to its use is the potential for toxic retinopathy. The incidence of hydroxychloroquine-induced retinopathy is low, but retinal damage is irreversible and may progress even after cessation of the drug.[2–4] The American Academy of Ophthalmology (AAO) has highlighted daily dosage, duration of use, renal disease, concomitant tamoxifen use, and coexisting macular disease as entities that are associated with increased risk of toxic retinopathy. In addition, a key component to limiting retinal toxicity is the regular ophthalmic screening of patients taking hydroxychloroquine with the goal of early detection of toxicity to preserve central vision. Current guidelines from the AAO provide best practices for screening for hydroxychloroquine retinopathy and recommend specific subjective and objective tests that have demonstrated sensitivity in detecting early toxicity.[5–8]

Several investigations of hydroxychloroquine toxicity screening have used spectral-domain optical coherence tomography (SD-OCT) in detecting anatomic changes present in hydroxychloroquine retinopathy.[9–12] The AAO recommends qualitative inspection of the SD-OCT B-scans for evidence of paracentral disruption of the ellipsoid band, as this has been found to correlate with a number of other functional measures of hydroxychloroquine-induced retinal changes.[4,6,13,14] Quantitative analysis of the retinal thickness measurements on SD-OCT by de Sisternes et al.[15] identified outer retinal thinning as a primary feature of hydroxychloroquine retinopathy. A recent study by Lally et al.[12] used a toxicity grading system that relied on trained graders at an OCT reading center to identify aspects of the foveal B-scan, including decreased reflectivity of the ellipsoid zone (EZ), disruption of the EZ, disruption of the interdigitation zone (IZ), disruption of the RPE, disruption of the external limiting membrane, and thinning of the outer nuclear layer (ONL). They reported that some of the earliest OCT changes in eyes with early toxicity were qualitative thinning of the ONL.[12] Another study demonstrated that SD-OCT–deter-

mined retinal thickness measured in specific Early Treatment Diabetic Retinopathy Study (ETDRS) subfields can be used to detect toxicity with high sensitivity and specificity.[16] Measurement of total retinal thickness is an accessible and helpful indicator but could potentially deemphasize retinal changes that are in the ONL in their earliest state.

A noninvasive and novel approach to harness different information present in OCT that can be exquisitely sensitive to outer retina changes was introduced with the development of the minimum intensity (MI) analysis of Cirrus SD-OCT (Carl Zeiss Meditec, Inc., Dublin, CA, USA). The MI measurement involves postacquisition analysis of each A-scan to identify the lowest image intensity value in the region between the inner limiting membrane (ILM) and RPE.[17] In normal retinas, ONL or Henle fiber layer (HFL) is the darkest layer and therefore harbors the MI value. In degenerative retinal diseases, such as geographic atrophy, in which the retinal architecture is altered in the outer retina, the OCT reflectivity of the ONL and HFL changes, and the MI values increase. The regions of abnormal MI values are coincident with those areas with abnormal ONL and HFL retinal architecture.[17]

In this study, we compare OCT-MI measurements in patients who have objective signs of hydroxychloroquine toxicity with patients who have been on long-term hydroxychloroquine but do not demonstrate toxicity. Based on this comparison, we consider whether OCT-MI measurements can contribute additionally to current screening procedures for detecting hydroxychloroquine-induced retinal toxicity in at-risk patients.

Methods

Study Participants

This prospective case-control study was conducted at the eye clinic of the National Eye Institute (National Institutes of Health, Bethesda, MD, USA). Inclusion criteria included a current or previous history of hydroxychloroquine treatment for a total duration exceeding 5 years and an absence of concomitant retinal disorders (e.g., diabetic retinopathy, retinal vein occlusion, AMD, or Stargardt's disease). Information on patient characteristics, including demographics, medical history, body weight and height, and duration and cumulative dose of hydroxychloroquine therapy, and diagnostic indications for hydroxychloroquine treatment, were obtained by medical history evaluation. The study protocol and informed consent forms were approved by a National Institutes of Health–based institutional review board and the study was registered at www.clinicaltrials.gov (identifier, NCT01145196). All study participants provided signed informed consent. The study protocol adhered to the tenets of the Declaration of Helsinki and complied with the Health Insurance Portability and Accountability Act.

Study Procedures

All participants underwent a comprehensive ocular examination, including best-corrected visual acuity testing using the ETDRS protocol, slit-lamp examination, and dilated fundus examination. In addition, all patients underwent multifocal electroretinographic (mfERG) testing, automated visual field testing, and retinal imaging, including SD-OCT, fundus autofluorescence (FAF) imaging, and color fundus photography. Testing was performed in both eyes of all participants. Because previous analyses demonstrated that structural and functional parameters are highly correlated between eyes,[16] only one eye per participant was used for statistical analyses and the right eye was arbitrarily chosen.

Visual Field Testing and Analysis

Perimetric assessment was performed using a standard 10-2 Humphrey Visual Field (HVF) Analyzer (Carl Zeiss Meditec, Inc.) with a white test spot. The visual field mean deviation (VFMD) values, representing deviation from age-matched normal eyes, were obtained from the visual field output.

mfERG Testing and Analysis

mfERG testing was performed according to the International Society for Clinical Electrophysiology of Vision guidelines,[18] based on the 61-hexagon stimulus pattern of the VERIS Clinic system (Electro-Diagnostic Imaging, Inc., Redwood, CA, USA). The 61 hexagon responses were grouped into five concentric rings (R1–R5). The average amplitude was assessed for each ring outside the R1 hexagon. The average response densities (nanovolts per degrees squared) within concentric rings from the center (ring 1) to the periphery (ring 5) were generated by the mfERG VERIS software. The ring ratios of the mfERG were defined as ratios of the central hexagon amplitude (R1) to each of the peripheral ring amplitudes (R2–R5). These ratios were calculated for all tested eyes. Participants were divided into two groups according to the presence (affected group) or absence (unaffected group) of hydroxychloroquine-related toxicity using objective mfERG criteria as previously described.[16] The presence of either of the following two conditions: (1) increased R1-to-R2 ratio (defined as exceeding the 99% confidence limits for the normal population), or (2) reduced R1 absolute amplitude (defined as less than the 99% confidence limits for the normal population) would designate the participant as having toxicity.[19] All remaining participants were assigned to the unaffected group. These objective criteria identified 19 affected participants and 38 unaffected participants in this cohort.[16]

SD-OCT Imaging and Analysis

Foveal-centered SD-OCT volumes were obtained for both eyes from each participant on the Cirrus-HD system (Carl Zeiss Meditec, Inc.) using the macular cube 512×128 scan pattern. The macular thickness map was divided into three concentric circles based on the ETDRS grading grid: a central circle (0.5 mm or 1.5° radius) centered on the fovea, a concentric inner ring (1.5 mm or 5° radius), and a concentric outer ring (3 mm or 10° radius). Radii at 45° and 135° angles were used to divide the circles into the nine ETDRS subfields: the central subfield and four inner and four outer subfields (temporal, superior, nasal, and inferior subfields). Mean retinal thicknesses in each of the nine subfields were generated by the manufacturer's software version 6.5.0.772 (Carl Zeiss Meditec, Inc.).

The OCT images also were acquired in parallel using the Heidelberg Spectralis HRA and OCT system (Spectralis; Heidelberg Engineering, Heidelberg, Germany). Horizontal 30-degree images through the fovea with 100 scans averaged were graded manually for the presence or absence of anatomic disruptions in the perifoveal EZ (i.e., the mitochondrial-rich layer near the inner segment–outer segment junction) located approximately 0.5 to 1.0 mm from the fovea. In cases in which the quality of Spectralis images was insufficient to visualize this region clearly (3 of 57 participants), corresponding Cirrus HD-OCT images were graded in their place. Two independent readers performed the grading in a masked fashion as previously described.[16]

Investigative Ophthalmology & Visual Science

Obtaining MI Values and Projection

The main purpose of the MI algorithm is to identify the minimum value of brightness along each A-scan between the ILM and RPE, which in normal retinas is located in the ONL, the site of photoreceptor nuclear bodies, as demonstrated in histologic correlate studies of OCT,[20,21] or the HFL, which appears approximately as dark as the ONL as long as the fibers are not oriented nearly perpendicular to the optical axis.[22] The general principles of MI processing have been described previously,[23–25] but also are described here.

The Cirrus macular cube 512 × 128 OCT scan was first segmented using the ILM and RPE segmentation algorithms used in the Cirrus analysis system. A speckle reduction algorithm was then applied to the image volume to remove background noise. The prototype speckle reduction used for this work consisted of an axial 11-point median filter (21 μm depth) followed by lateral smoothing using a Hamming window of 11 pixels width (130 μm width). The design of the speckle reduction is not extremely critical and involves choosing tradeoffs among noise reduction, lateral resolution, and axial resolution; a different variation of the MI image processing has also been successfully used by Niu et al.[26]

Logarithmically transformed image data were used as an input to the speckle reduction. Because the log transformation does not change the ordering of the data, the axial median filtering is not affected by the log mapping; values are of course different, but the same pixels are selected as the medians as long as the mapping is monotonic. For the lateral speckle reduction smoothing, the log mapping will decrease the relative contributions from higher intensities to the result, so that edges may appear less sharp. This would not affect the detection of minima, though. If the lateral values of the image volume at a given depth z are $x(i,z)$ and the Hamming window is denoted by $h(j)$, the result of the lateral smoothing is:

$$y(i,z) = \sum_{j=1}^{11} h(j)x(i-j,z). \quad (1)$$

At the MI of the smoothed image at lateral location i, the result at $z_{\min}$ is less than it is at all other depths z:

$$\begin{aligned} y(i,z) &= \sum_{j=1}^{11} h(j)x(i-j,z) > y(i,z_{\min}) \\ &= \sum_{j=1}^{11} h(j)x(i-j,z_{\min}), \quad \forall z \neq z_{\min}. \end{aligned} \quad (2)$$

The difference between each smoothed image and its minimum is given by:

$$y(i,z) - y(i,z_{\min}) = \sum_{j=1}^{11} h(j)[x(i-j,z) - x(i-j,z_{\min})] > 0, \quad \forall z \neq z_{\min}. \quad (3)$$

If the data are logarithmically transformed, the sign of each of the bracketed terms does not change because the transformation is monotonic:

$$\sum_{j=1}^{11} h(j)\{\log[x(i-j,z)] - \log[x(i-j,z_{\min})]\} > 0, \quad \forall z \neq z_{\min}. \quad (4)$$

So, the inequality is still true after the logarithmic mapping, and the location of the minimum is unchanged by that transformation. For the subfield averaging used in later analysis, the median is used. The ordering of the data is unchanged by the monotonic transformation, so any comparisons between median values are unaffected by the transformation.

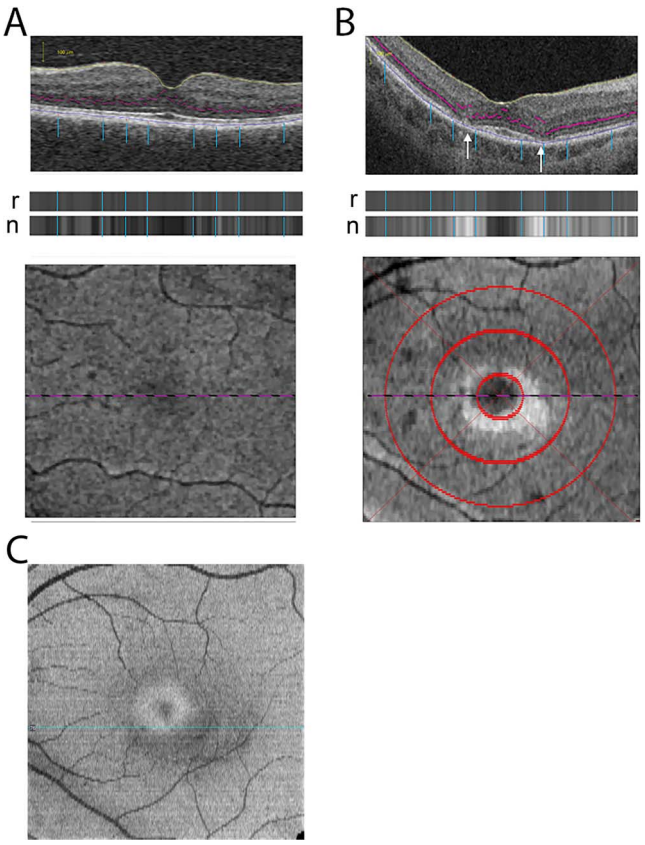

Figure 1. Quantitative analysis of MI signal in each SD-OCT (6 × 6 mm, 512 × 128) scan. (**A**) Unaffected retina. (*Top*) Intensity levels (i.e., gray levels) of individual pixels in each A-scan are computed, and the lowest, or minimum, intensity pixel (as depicted by a *purple circle*) identified and its gray level recorded (raw MI value). (*Middle*) The *darkest pixels*, termed the minima, from each A-scan were collected into a 2D line representing the B-scan. *Blue lines* indicate relative position of the minima on the B-scan shown in the 2D representation of the collected minima. *Top band* are the raw values (labeled r) and the *bottom band* represents the normalized values (labeled n). (*Bottom*) Each of the 128 horizontal lines of minima are then compiled into en face image called an MI projection. The *dotted line* on the en face image indicates the position of the B-scan shown in the upper panel. (**B**) Similar depictions are shown for a study eye in the affected group. (*Top*) A-scans traversing areas of outer retinal disruption typical of hydroxychloroquine toxicity demonstrate higher MI values than observed in unaffected study eyes (*white arrows*). (*Middle*) The 2D representation of the MI for the B-scan (raw MI) is shown (labeled r) with the panel below indicating the normalized MI values of the same B-scan (labeled n). (*Bottom*) In the assembled en face projection image, these areas appear as having elevated intensities (brighter) in the inner retinal subfields. *Red circles* represent the borders of the ETDRS grid with diameters of 1 mm, 2 mm, and 3 mm. Median minimum intensities are calculated for each ETDRS subfield in later analyses. (**C**) Using the Cirrus software to generate automated segmentation of the retinal layers, the EZ band was extracted from the OCT of a study eye in the affected group (same scan used in Fig. 1B) to create an en face image of the EZ band. The en face OCT image reveals parafoveal concentric zone of reduced reflectivity from the EZ zone.

After speckle reduction, the pixel of lowest intensity between the ILM and RPE boundaries was identified. In normal unaffected areas of the retina, the minima of the intensity will be located within the ONL or HFL (Fig. 1A, purple circles). These minima were collected into a one-dimensional line corresponding to the B-scan, and the lines from each B-scan were then compiled into a two-dimensional (2D) en face image, called the MI projection (Fig. 1A). The reflectivity of the

ONL may be increased in certain outer retina pathologies. In hydroxychloroquine retinopathy, the reflectivity of the ONL of the parafoveal macula is increased, as visualized by the B-scan in Figure 1B, and the minima may be displaced to the inner retina (Fig. 1B, white arrows).

Raw MI Values and Normalized MI Values

Applying these algorithms to the OCT A-scan, the MI can be determined and quantitatively analyzed. This quantitative MI value for each A-scan was derived in two different ways. One algorithm recorded the absolute/raw intensity value of the lowest intensity pixel in the A-scan (raw MI). The other algorithm derived a corrected intensity value of the minimum intensity pixel following normalization to intensity values from the overall scanning field (normalized MI) so as to correct for the contributions of variations in signal (i.e., cataracts or vitreous opacities) that can affect the scan intensity. The effect of normalization can be visualized in the 2D reconstruction in the second bands of the example in Figure 1, middle panels. The normalization is performed using a "trimmed mean" en face image, created from the mean of 70th to 95th percentile intensities, which is then blurred with a circular smoothing function of 0.5-mm diameter. The choice of intensity percentiles was intended to exclude the effects of moderate amounts of dark fluid or hyperreflective material. An offset of 20 grayscale units is added to the blurred "trimmed mean" en face image to moderate the effect of the normalization. The raw MI image (r) is divided by this normalization image to give the normalized MI (represented by the horizontal line labeled "n" in Figs. 1A, 1B). The blue lines on each of B-scans indicates which areas on the B-scan are responsible for generating the value depicted in the 2D reconstruction of the raw and normalized MI values for the example B-scans.

Minima from each of the 128 B-scans from the macular cube were assembled into horizontal lines and then compiled into a 2D en face image called an MI projection (Fig. 1, bottom). In Figure 1A, normal retina demonstrates minima in the ONL and HFL that appear gray in an en face 2D image. Figure 1B demonstrates the MI projection from a 6×6-mm macular OCT scan on a patient with documented hydroxychloroquine retinopathy. As each pixel represents a minimum intensity value depicted in grayscale, the region of increased MI around the fovea is apparent in the Minimum Intensity Projection image of this example as a white ring where minimum intensities are greater relative to the surrounding retina (gray).

A specific finding in hydroxychloroquine retinopathy is disruption of localized EZ band on qualitative inspection of the SD-OCT.[6] Using automated segmentation software on the Cirrus-HD system to detect the EZ band, Figure 1C demonstrates the en face OCT image on a patient (same patient used to generate Fig. 1B) with documented hydroxychloroquine retinopathy and reveals a parafoveal zone of reduced reflectivity in the EZ.

Quantitative Analysis of the MI Value

MI values were generated for all A-scans in the macular cube 512×128 scan. The median MI value (MI_{median}) across each of the nine ETDRS OCT subfields (central subfield and the four inner and four outer subfields [superior, nasal, inferior, and temporal subfields]) were obtained and used for statistical analysis. Results of right and left eye MI_{median} values in each OCT subfield were compared for each participant. Nonparametric Spearman correlation coefficients were calculated for each comparison.

MI_{median} values for each OCT subfield were compared between the group affected with hydroxychloroquine-induced toxicity and those unaffected using a nonparametric *U*-test (Mann-Whitney). MI_{median} values were obtained with the "raw" applied algorithm (raw MI_{median}) as well as with the normalization algorithm (normalized MI_{median}).

To determine how well the MI_{median} measurement discriminated between affected and unaffected participants, we used a cross-validation approach.[27] A random number generator was used to divide the study population into two subsamples. For MI_{median} values from each OCT subfield, we computed the area under the receiver operating characteristic (ROC) curve to identify the cut-point associated with Youden's J statistic, an index that identifies as optimal the point on the ROC curve that is farthest from chance.[28] The optimal MI_{median} cut-point identified from the first subsample then was applied to the second subsample, and the sensitivity and specificity were determined in the second subsample.

Results

Study Participant Characteristics

The mean age of the study participants was 55.7 ± 10.7 years (range, 31–72). Females comprised most participants (91%) and the mean duration of hydroxychloroquine treatment was 15.0 ± 7.5 years.[16] mfERG testing was performed on all 57 participants, and previously published values for R1 amplitudes and R1-R2 ratios[19] were used to classify the patients as being either unaffected or affected by hydroxychloroquine retinopathy. As previously described in a study by our group using the same patient sample,[16] 19 participants had at least one eye falling outside the mfERG limits and were classified as the affected group (16 participants meeting criteria in both eyes, 3 participants meeting criteria in one eye). The remaining 38 participants did not have either eye meeting the toxicity criteria and were classified as unaffected.

The demographic and ocular characteristics for the cohorts have been previously presented[16] and are summarized here in Table 1 and Table 2, respectively. There was no statistically significant difference between the affected and unaffected groups with regard to mean age, sex, or indication for treatment ($P > 0.05$ for all comparisons). However, the affected group did have a higher proportion of participants older than 60 years (58% versus 29%) and the difference met the condition for statistical significance ($P = 0.05$). In addition, factors that have previously been associated with increasing risk of hydroxychloroquine toxicity[29,30] did not differ significantly between the two groups, including length of treatment duration ($P = 0.54$), cumulative dose ($P = 0.71$), and daily dose in mg/kg real weight ($P = 0.77$).

Measures of visual acuity and automated visual field testing were significantly different between affected and unaffected groups (Table 1). Mean visual acuities in participants' right eye (the designated study eye in each participant) were 85.3 ± 5.8 letters (≈20/20) in the unaffected group, compared with 77.4 ± 12.4 letters (≈20/32) in the affected group ($P = 0.001$). Mean deviation as computed from the HVF 10-2 was significantly lower in the affected group (–12.3 ± 8.8 dB right eye) compared with the unaffected group (–0.8 ± 1.5 dB right eye) ($P < 0.0001$).

Median MI

The SD-OCT macular cube images were assessed and the MI algorithms were applied postacquisition. For all patients, raw generated MI values and normalized MI values were calculated for all A-scans in the acquired OCTs. A median MI value from the raw MI analysis (raw MI_{median}) and from the normalized MI

Table 1. Participant Demographics

	Retinopathy, $n = 19$	Without Retinopathy, $n = 38$	P
Age, y, mean ± SD	58.8 ± 10.0	54.1 ± 10.4	0.13
Patients older than 60, n (%)	11 (58)	11 (29)	0.05
Sex, female	18 (94.7)	34 (89.5)	0.66
Total cumulative hydroxychloroquine dose, g, mean ± SD	1871 ± 927	2036 ± 1141	0.71
Length of treatment, y, mean ± SD	15.3 ± 7.1	14.9 ± 8.3	0.54
Height, cm	159.6 ± 6.9	157.8 ± 10.9	0.3037
Weight, kg	71.9 ± 30.9	71.9 ± 17.7	0.1607
Daily dose, mg/kg ideal body weight/d	6.84 ± 1.60	7.96 ± 2.20	0.063
Daily dose, mg/kg real body weight/d	5.61 ± 2.03	5.51 ± 1.41	0.77
Indication for hydroxychloroquine use, n (%)			1.00
Lupus	12 (63.2)	24 (63.2)	
Rheumatoid arthritis	6 (31.6)	12 (31.6)	
Sjögren syndrome	1 (5.3)	2 (5.3)	

analysis (normalized MI_{median}) were generated for each subfield of the ETDRS grid centered on the fovea. Although all other previously analyzed measures of retina structure and function demonstrated high correlation between eyes in a prior study,[16] we examined the interocular correlation of MI_{median} values for each OCT subfield. Examining all eyes, for all subfields, with both the raw MI algorithm and the normalized MI algorithm, we found a high correlation between MI_{median} values in the right and left eyes. Correlation coefficients were higher with the normalized MI algorithm than the raw MI algorithm, with correlation coefficients for normalized MI ranging from $r = 0.80$ in the center subfield to $r = 0.91$ in the inner inferior subfield (Fig. 2) ($P < 0.0001$ for all) and raw MI correlations ranging from 0.56 to 0.7 ($P < 0.0001$ for all). Right eyes are used as the designated study eye for each participant in subsequent analyses.

Scatter box plots of the MI_{median} for each of the nine macular OCT ETDRS subfields are displayed in Figure 3 for affected ($n = 19$) and unaffected ($n = 38$) for both raw MI_{median} values and normalized MI_{median} values. For all comparisions, MI_{median} values were statistically higher for the affected group compared with the unaffected group; this was true for comparisons for all nine OCT subfields and for both the raw and normalized MI_{median} values. The OCT subfield with the greatest difference in the median MI_{median} between the affected and unaffected groups was the inner inferior subfield (normalized: affected median $MI_{median} = 57.30$, unaffected median $MI_{median} = 46.75$, $P < 0.0001$; raw: affected median $MI_{median} = 69.00$, unaffected median $MI_{median} = 55.50$, $P < 0.0001$). In all inner subfields, the normalized MI analysis has fewer data points from each study group that lie in the interval common to the ranges for both group distributions (i.e., overlap between groups). The normalized MI analysis is the MI analysis used for the remainder of the analyses presented.

Performance of MI Technique as Screening Tool

We assessed the ability of OCT-MI technique to detect hydroxychloroquine retinopathy using a cross-validation approach. The study population was divided randomly into two subsamples: subsample 1, consisting of 10 affected and 19 unaffected eyes/participants, was first used as a training set, and subsample 2, consisting of 9 affected and 19 unaffected eyes/participants, was used as a validation set. The ROC, area under the curve (AUC), and Youden's J statistic were calculated for each parameter in the training set. The optimal cutoff was applied to the validation set to determine its performance. Table 3 shows the optimal cutoff for each parameter in the first subsample and the performance of the second subsample. For example, using Youden's J statistic for the inner inferior subfield MI_{median}, the optimal cutoff for the training set was 51.70 (AUC = 1.00; sensitivity = 100%, confidence interval [CI] 69%–100%; specificity = 100%, CI 82%–100%) (Fig. 4A). When this cutoff point was applied to the validation set, similar results were obtained: of 9 affected patients, 8 were identified correctly (sensitivity = 89%), and of 19 unaffected patients, 18

Table 2. Participant Ocular Characteristics

	Retinopathy, $n = 19$	Without Retinopathy, $n = 38$	P
Mean Snellen visual acuity right eye (range)	20/32 (20/16–20/200)	20/20 (20/12.5–20/63)	
Mean letters right eye, mean ± SD	77.4 ± 12.4	85.3 ± 5.8	0.001
Mean mfERG R1 OD	43.5 + 33.7	86.0 + 25.2	<0.0001
Mean mfERG R1/R2 OD	2.9 + 2.0	1.9 + 0.26	0.0005
HVF mean deviation OD, mean ± SD	−12.3 ± 8.8	−0.8 ± 1.5	<0.0001
OCT ETDRS subfield thickness OD			
Center, µm, mean ± SD	208.3 + 49.3	248.5 + 37.4	
Inner superior subfield, µm, mean ± SD	263.7 + 35.5	316.4 + 17.8	<0.0001
Inner nasal subfield, µm, mean ± SD	260.5 + 33.9	317.3 + 20.1	<0.0001
Inner inferior subfield, µm, mean ± SD	251.7 + 32.6	311.1 + 19.3	<0.0001
Inner temporal subfield, µm, mean ± SD	240.5 + 32.9	302.5 + 19.5	<0.0001
Outer temporal subfield, µm, mean ± SD	232.8 + 30.5	277.6 + 15.7	<0.0001
Outer nasal subfield, µm, mean ± SD	240.2 + 36.1	291.8 + 18.6	<0.0001
Outer inferior subfield, µm, mean ± SD	215.6 + 33.5	263.8 + 15.2	<0.0001
Outer temporal subfield, µm, mean ± SD	203.6 + 30.6	257.9 + 22.9	<0.0001
OCT Photoreceptor IS/OS disruption OD, n (%)	16 (84)	0 (0)	<0.0001

Investigative Ophthalmology & Visual Science

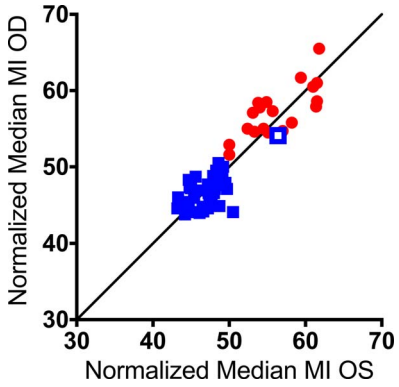

FIGURE 2. Correlation between eyes of normalized MI_{median} of the inner inferior subfield. Normalized MI_{median} of the inner inferior subfield of the right eye plotted against normalized MI_{median} of the inner inferior subfield of the left eye of each participant (unaffected: *blue squares*; affected: *red circles*; individual in *open blue squares* is discussed in the case study section). A line of identity with slope = 1 through *y*-intercept of 0 is present for reference. Spearman coefficient $r = 0.91$ ($P < 0.0001$).

were identified correctly (specificity = 95%) (Fig. 4B). When this analysis was performed in the reverse order with subsample 2 as the training subset, the optimal cutoff point for inner inferior subfield MI_{median} was found to be 50.65 (AUC = 0.99; sensitivity = 100%, CI 66%–100%; specificity = 95%, CI 74%–100%) (Fig. 4C). Applied to subsample 1 for validation, affected patients were fully identified: all 10 subjects with toxicity were identified correctly (sensitivity = 100%), and all 19 unaffected patients were identified correctly (specificity = 100%) (Fig. 4D).

Although the left eyes of our study population do not represent an independent data set, we observed the performance of the left eyes by applying cutoff values determined from the right eyes. The optimal cutoff values for all right eyes, right eye subsample 1, and right eye subsample 2 of the inner inferior subfield were MI_{median} = 51.05, 51.70, and 50.65, respectively. These cutoff points were then applied to the inner inferior subfield of left eyes and they all performed equally well (sensitivity = 90% and specificity = 97% for all three cutoff values).

Comparison of OCT-MI Evaluation to OCT Thickness Measurements and to Visual Field Measurements as Assessments for Toxicity Screening

We plotted the distributions of MI_{median} values obtained from the inner inferior subfield in patients with and without toxicity and compared them with the corresponding distributions of SD-OCT–derived total retinal thickness measurements and mean sensitivity deviations (MD) for HVF 10-2 testing for the same groups and retinal location (Fig. 5A, 5B). For each modality, participants with measurements that were located in the region of overlap between the two distributions (i.e., with and without toxicity) were highlighted (with a black box) and enumerated. In the MI analysis, only 3 participants (5.2%) of 57 were located in the region of overlap, compared with 20 (35%) of 57 for OCT retinal thickness measurements, and 24 (61%) of 55 for HVF sensitivity measurements. These comparisons indicate that MI measurements can perform well in separating patients with and without toxicity, at a level comparable, or even superior to, other more established modalities. Comparison of the corresponding ROC curves for each of the three modalities also highlight MI analysis as being capable of high sensitivity and specificity, comparing favorably with OCT thickness and HVF 10-2 MD measurements.

Patients With mfERG Values Meeting Threshold in One Eye Only

Our criteria for determining the presence or absence of toxicity in our cohorts were the published threshold values on normal mfERG ring amplitudes and ring-to-ring ratios.[19] From the 19 patients who we classified as affected, 16 met the mfERG criteria for toxicity in both eyes. Of the three patients who did not meet classification on mfERG in both eyes, two patients (subjects 009 and 017) surpassed threshold values in the left eye only and one patient met criteria for toxicity in the right eye only (subject 011). These three patients warranted a closer look.

Evaluation of their eyes using HVF 10-2, qualitative and quantitative analysis of SD-OCT, color fundus photography, and FAF demonstrated clinical evidence of toxicity in both eyes of these three patients, and the results were highly correlated between both eyes on all parameters tested (e.g., VFMD, severity on FAF grading scale, macular thickness of inner inferior subfield on SD-OCT). We classified these three patients as "affected" in both eyes and segregated them into the affected cohort. As described in our methods, we arbitrarily selected to use only the right eye of our patients for all analyses performed on OCT-MI.

Examining our subfield of interest, the inner inferior subfield, the MI values in the right eye for patients 009, 011, and 017 were MI_{median} = 58.5, 54.6, and 57.8, respectively (affected median MI_{median} = 57.3, unaffected median MI_{median} = 46.75). For the left eyes of patients 009, 011, and 017, the MI_{median} = 54.9, 53.3, and 54.0, respectively (affected median MI_{median} = 55.1, unaffected median MI_{median} = 47.25). Although the mfERG values were equivocal for one eye in each of the three patients in defining toxicity, the MI analyses on both eyes of these patients demonstrated MI values that were higher and would segregate with the affected cohort when evaluating the MI values of the inner inferior subfield. This case series may also lend value to the robustness of the MI analysis for detecting this pathology.

Case Study

Although this study was a cross-sectional analysis, we did observe one particular study participant whose initial testing led her to be assigned to the "without toxicity group" based on objective mfERG criteria evaluated at the time of enrollment in the study (R1 central amplitudes 49.2 [OD] and 50.1 [OS] microvolts, R1/R2 ratios 1.5 [OD] and 2.1 [OS]). Despite this assignment at baseline, this participant demonstrated MI values that were higher than those of other patients in this unaffected cohort (Fig. 3, open blue squares). In the inner ETDRS ring, two of the four subfields for this patient revealed MI values that were located within the range of the distribution of MI values of patients with toxicity (Figs. 3D, 6C, open blue squares). Using MI criteria alone, this patient demonstrated values consistent with toxicity, in contradiction to the assignment by mfERG criteria.

This participant was seen at follow-up 36 months later where she demonstrated changes that met criteria for toxicity (Fig. 6B), which had been heralded by MI measurements at baseline. At the follow-up visit, the MI measurements in four of the four inner subfields were now clearly within the toxicity range (Fig. 6C, red open squares). This case example suggests that MI measurements may dynamically increase in different retinal locations during early emergence of clinically evident toxicity. The development of these dynamic increases in MI may potentially precede the assignment of the toxic status as defined by mfERG criteria.

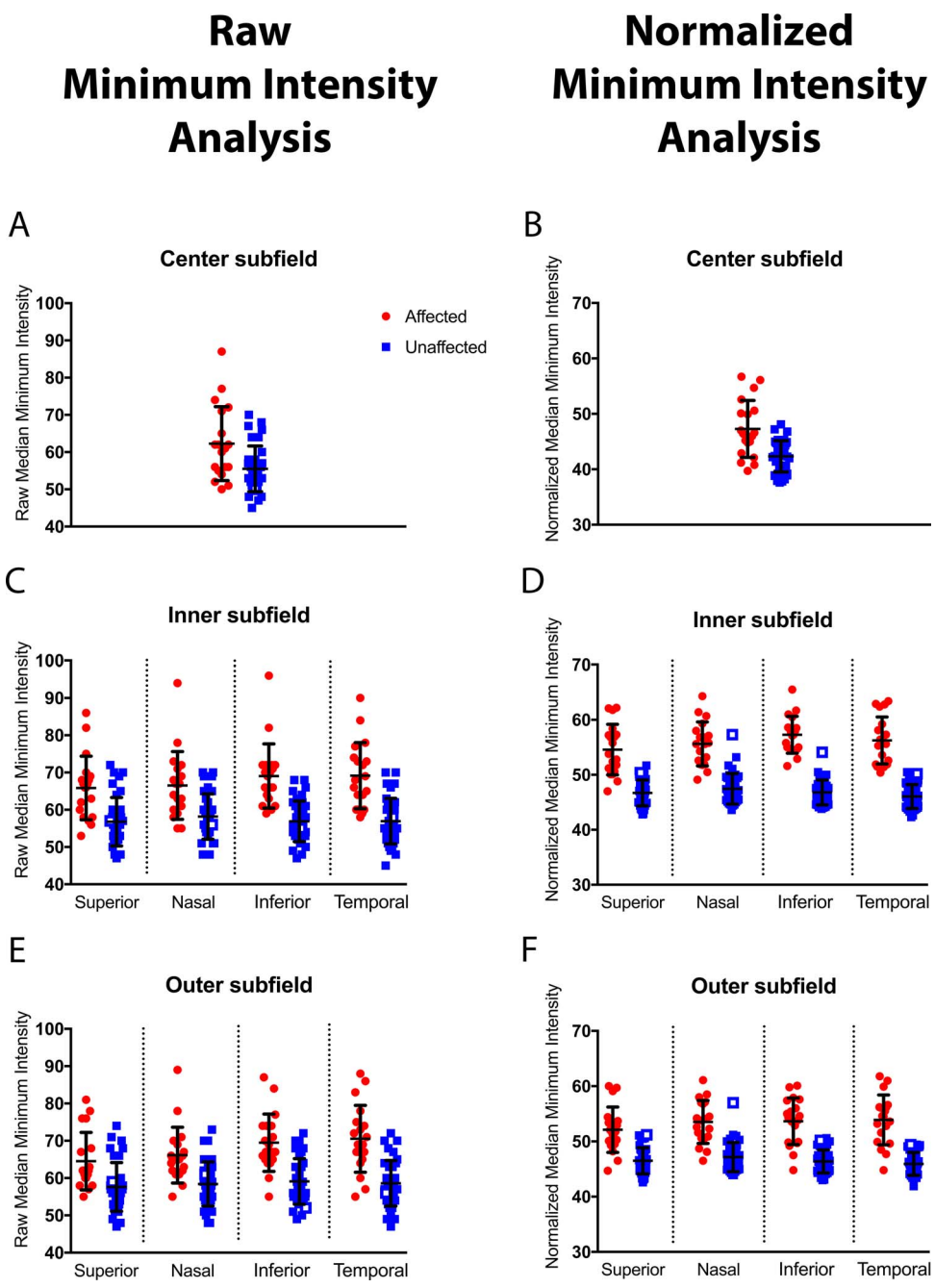

Figure 3. Comparison of median MI between affected and unaffected study eyes by retinal subfield. The MI values of all A-scans were calculated for each study eye (right eye of each participant) and the median MI within each OCT subfield was compared between the affected and unaffected participant groups (i.e., each point depicted represents the median intensity value for a single study eye for that particular subfield; the *midpoint* and limits of the *error bars* indicate mean and SD, respectively). MI values were calculated without (i.e., "raw" values) (**A**, **C**, **E**) and following a normalization algorithm (i.e., "normalized") (**B**, **D**, **F**) for each of the nine subfields. Individual in *open blue squares* is discussed in the case study section.

Discussion

This is the first report using MI analysis in studying hydroxychloroquine toxicity, as well as for investigating its potential for use as a screening tool. Patients in this study were extensively characterized by all the recommended testing by the AAO guidelines and were classified as having or not having hydroxychloroquine retinopathy by using objective mfERG criteria. Among the eyes with toxicity, additional modalities of screening also demonstrated abnormalities as previously reported.[16] Although other screening modalities, such as VFMD and OCT thicknesses have demonstrated good correlation with toxicity,[16] the MI analysis demonstrates almost perfect segregation with the affected status and has the higher AUC. As this method uses existing, and widely available technology and provides novel objective analysis that adds a new dimension to assess retinal pathology in vivo, it has the potential to be a useful addition to current screening modalities.

The OCT modality is widely used and included in the AAO's primary screening recommendations.[6] The AAO's discussion of

Investigative Ophthalmology & Visual Science

Table 3. ROC Curve Analysis of Random Half-Sampling of Data

	Training Set					Performance of Validation Set	
Parameter	**Youden's J Statistic**	**Optimal Cutoff Point**	**AUC**	**Sensitivity, %**	**Specificity, %**	**Sensitivity, %**	**Specificity, %**
Center	0.647	45.65	0.87	70	95	44	90
Inner S	0.804	49.65	0.96	90	89	89	84
Inner N	0.947	51.75	0.98	100	95	78	95
Inner I	1.000	51.70	1.00	100	100	89	95
Inner T	1.000	50.95	1.00	100	100	89	100
Outer S	0.542	48.95	0.80	70	84	100	84
Outer N	0.647	50.55	0.86	70	95	100	89
Outer I	0.695	49.55	0.88	80	89	89	95
Outer T	0.742	47.65	0.90	90	84	100	74
Full	0.595	48.85	0.86	70	89	100	84

examination of SD-OCT relies on qualitative inspection of local anatomic changes.[6] Although localized thinning of photoreceptor layer and disruption of the ellipsoid zone is a specific finding in hydroxychloroquine toxicity, it requires an educated reviewer, and previous studies have demonstrated that this finding alone is not always the most sensitive testing modality.[16] In a recent study by Lally et al.[12] using expert graders to examine structural changes on SD-OCT on eyes with early clinical signs of toxicity, the authors observed parafoveal ONL and IZ changes frequently in the absence of EZ disruption. This may suggest that ONL and IZ changes precede EZ disruption as the earliest signs of hydroxychloroquine toxicity. Although the MI projection (Fig. 1B) and the EZ en face (Fig. 1C) may both show disruption to the outer retinal anatomy in the parafoveal region, the MI projection reflects ONL disruption and the depiction of the disturbance may not match the en face of the EZ, especially in cases of early toxicity in which EZ disruption is not apparent. Studies employing trained readers at a reading center to grade qualitative thinning of the ONL have demonstrated utility in identifying toxicity.[12] The addition of an analysis that could provide a quantitative measure of OCT reflecting outer retinal changes would lessen the reliance on an expert interpretation, which would broaden its application as a screening test.

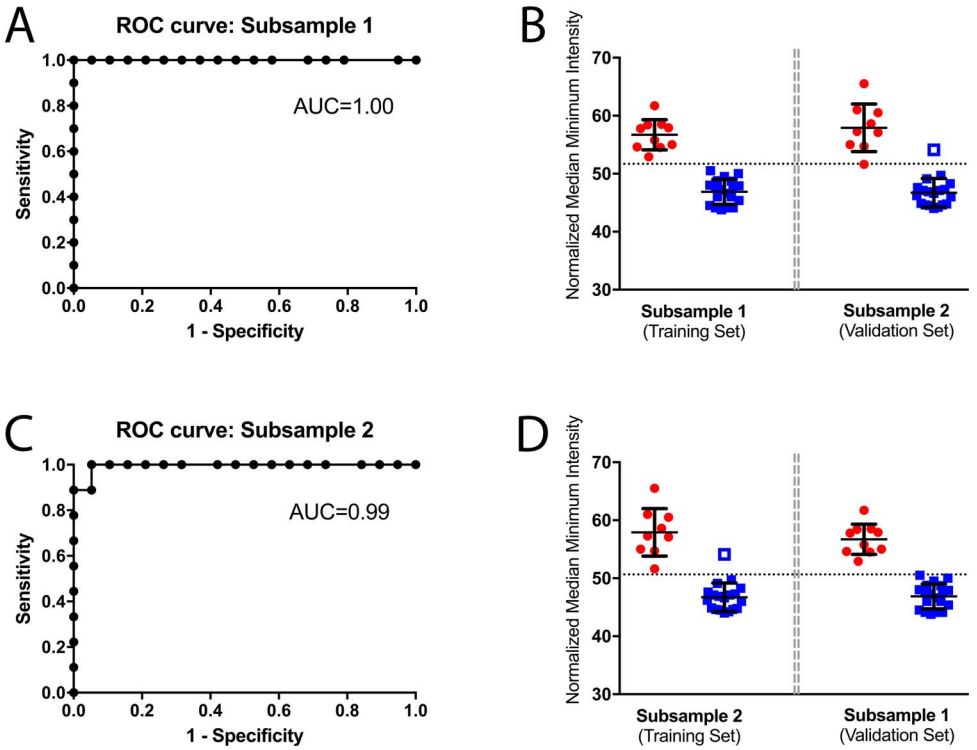

Figure 4. Cross-validation analysis for performance of the median minimum intensity value (MI_{median}) of the inner inferior ETDRS subfield in identifying hydroxychloroquine-induced toxicity. (**A**) Results of subsample 1 used as a training set for ROC curve analysis. (**B**) The calculation of the Youden's J statistic was used to determine a cutoff for MI value for the analysis of the inner inferior OCT subfield. Scatterplots of the MI_{median} for inner inferior subfields of study eyes in the affected (*red*) and unaffected (*blue*) groups with the identified cutoff value demonstrated in the *dashed line*. Subsample 2 serves as a validation set and demonstrates the performance of this cutoff value in discriminating between the cohorts. (**C**) Results of subsample 2 used as a training set for ROC curve analysis. Again, the calculation of the Youden's J statistic was used to determine a cutoff for MI value of the inner inferior OCT subfield. (**D**) Scatterplots of the MI_{median} for inner inferior subfields of study eyes in the affected (*red*) and unaffected (*blue*) groups with the identified cutoff value demonstrated in the dashed line. In this analysis, subsample 1 serves as a validation set and demonstrates the performance of this cutoff value in discriminating between the cohorts.

Investigative Ophthalmology & Visual Science

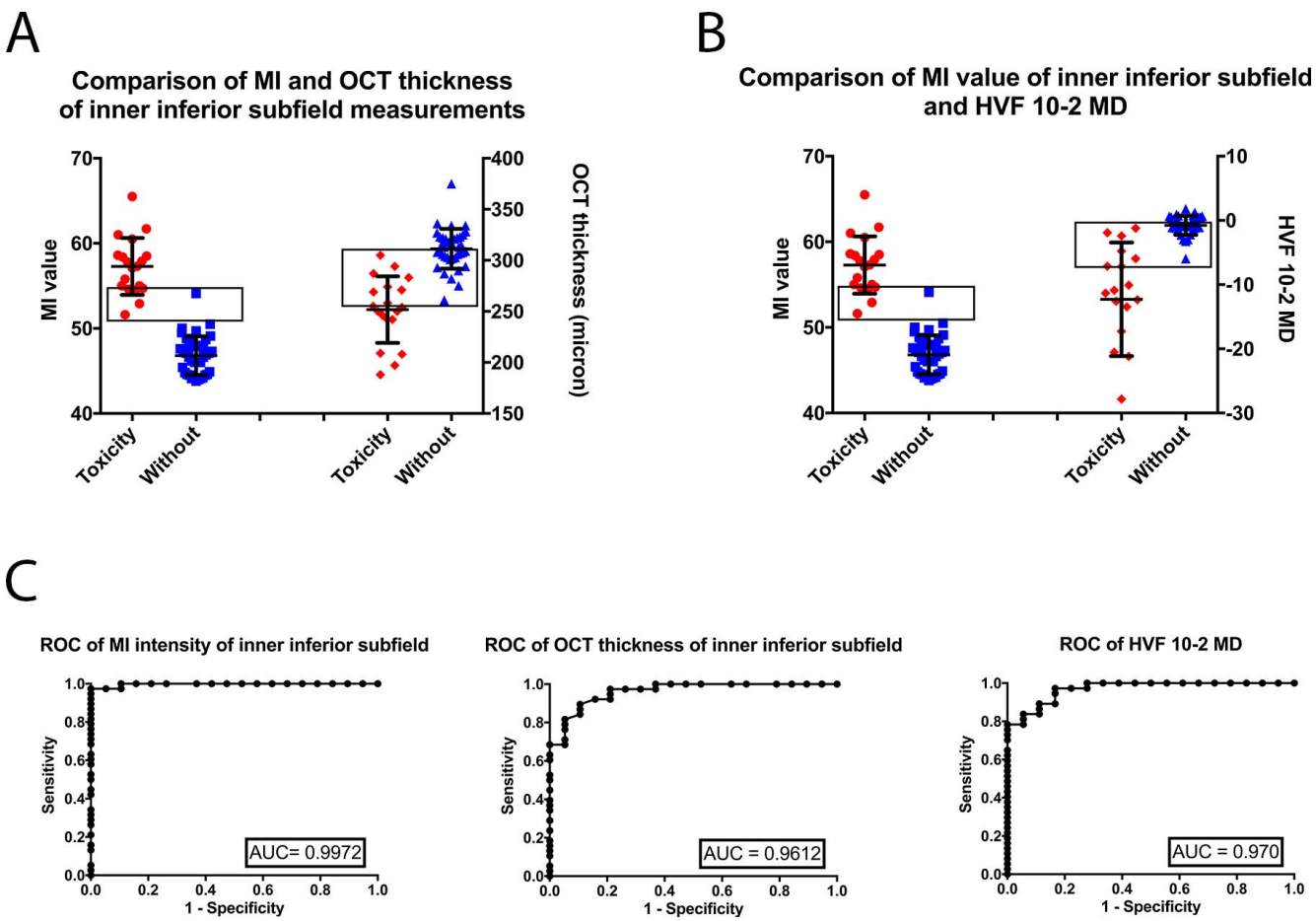

Figure 5. Comparison of clinical testing modalities. (**A**) The inner inferior subfield measurements for both MI values and OCT subfield thickness are compared for the affected and unaffected cohorts. The *black box* draws attention to the number of individuals who exist in the overlap range between the affected and unaffected groups for each test. (**B**) The inner inferior subfield MI measurements are compared with the HVF 10-2 for eyes in the affected and unaffected cohorts. The *black box* draws attention to the number of individuals who exist in the overlap range between the affected and unaffected groups for each test. (**C**) ROC curve plotted for MI values of the inner inferior subfield, OCT subfield thickness of the inner inferior subfield, and HVF 10-2 MD. AUC listed for each test. A test with 100% sensitivity and specificity would have an AUC of 1.0.

In our analysis, the inner inferior subfield MI_{median} analysis demonstrated the highest sensitivity and specificity in identifying eyes affected with hydroxychloroquine toxicity. The importance of this subfield in the detection of hydroxychloroquine toxicity echoes results of other observations about the geographic preference for the first changes induced by hydroxychloroquine.[8,13,16] What underlies this particular local sensitivity has yet to be understood, but the data here add to the evidence supporting the importance of this area in hydroxychloroquine screening.

As our role in hydroxychloroquine screening is aimed at determining the earliest demonstration of toxicity, our field would benefit from even more sensitive tests. Although the structure of this cross-sectional study cannot comment on relative sensitivities,[31,32] we do find an example of a case that initially was classified as not having toxicity per the standard panel of screening testing results, but did later progress to demonstrating evidence of hydroxychloroquine toxicity. By comparing performance on MI analysis at the two time points, we can appreciate that in this particular case, the MI_{median} subfield values at the initial time point appeared to be in the toxicity (i.e., affected) range in the inner inferior subfield and inner nasal subfield and may have been an early indication of structural changes that were harbingers of hydroxychloroquine toxicity even though the criteria used identified this patient as being unaffected.

An interesting observation and investigation from Lujan et al.[22] demonstrates that the reflectivity of the outer retina on OCT changes based on the incidence angle of the light through the pupil. Specifically, an offset entry beam may increase reflectivity of the HFL on one-half of the B-scan, and it may decrease the reflectivity of the HFL of the other half of the B-scan, making the reflectivity appear low and visually indistinguishable from the ONL.

Although we did not fully explore the possible effects of the SD-OCT beam entrance position on the MI values, a review of the scans in this study does not reveal a systematic horizontal offset (either between groups or in the direction of any tilt), and thus we do not believe this contributes to our overall results.[22] However, it is possible that the MI value could be affected by beam entry position and the magnitude of such an effect should be investigated further. We also must point out that the size of this data set is small and that these results must be replicated with an independent data set. Additional analyses of other data sets are necessary to validate this new analysis in demonstrating its potential utility as a screening modality in this disease.

The utility of MI analysis was demonstrated in patients with AMD to predict growth of geographic atrophy.[17] The MI

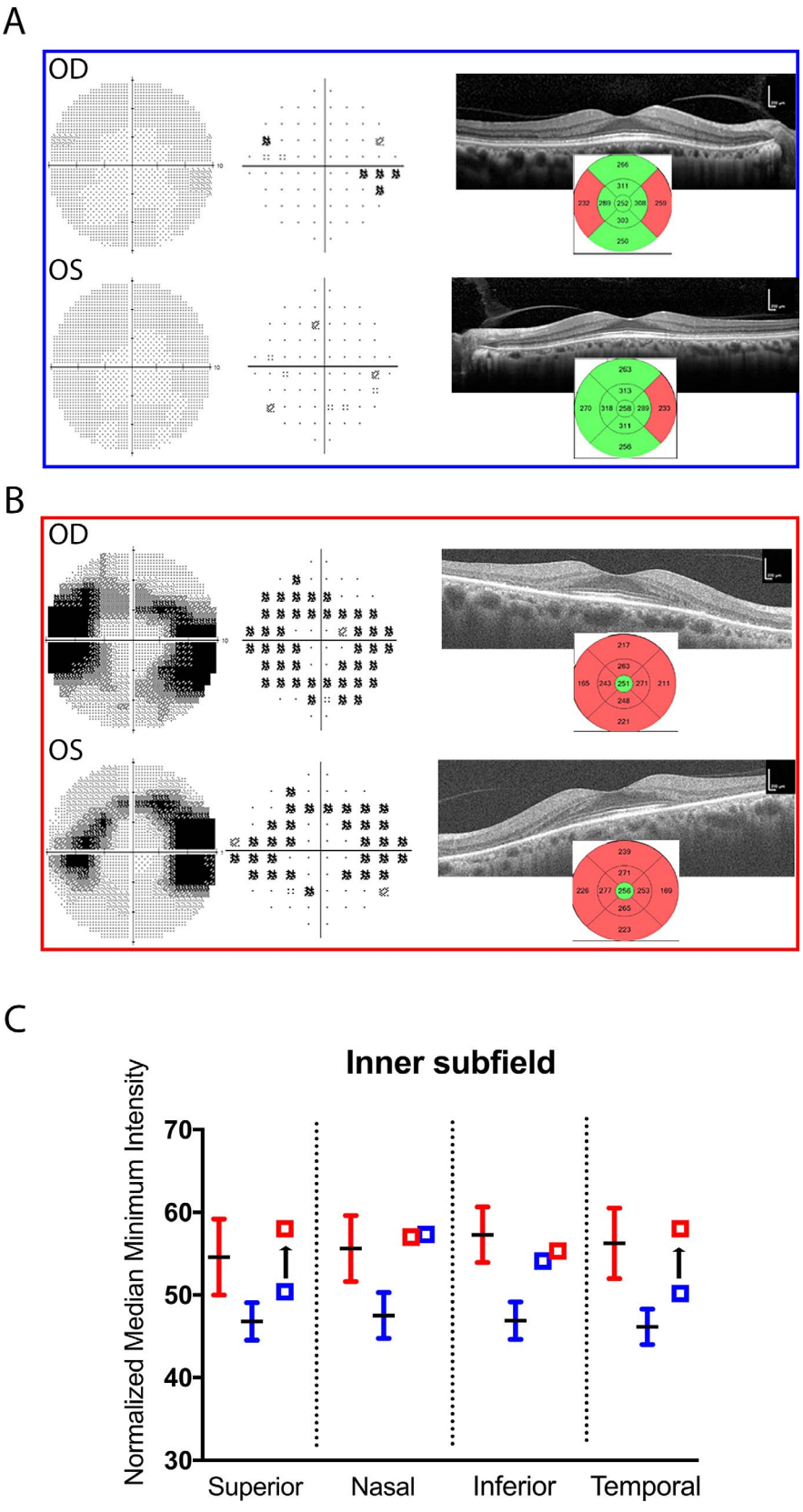

Figure 6. Case study of individual transitioning from unaffected group to affected status 3 years later. (**A**) HVF 10-2 visual field and OCT testing results in a participant meeting criteria for unaffected group at initial visit (MI values of this individual indicated in other figures with *open blue squares*). (**B**) After returning 3 years later, HVF 10-2 testing and OCT demonstrated changes consistent with hydroxychloroquine toxicity. (**C**) MI_{median} analysis in the inner subfields of this participant at initial visit (*open blue squares*) and follow-up 3 years later (*open red squares*). *Adjacent bars* indicate mean and SD MI_{median} values of affected (*red*) and unaffected (*blue*) groups for comparison.

Investigative Ophthalmology & Visual Science

analysis also may prove useful in demonstrating outer retinal loss in other degenerative retinal diseases. The nature of the MI analysis in reflecting structural changes in the outer retina that are consistent with disease pathogenesis makes this analysis a promising screening modality that could be a welcome addition to our current screening tools.

Acknowledgments

Supported by the National Eye Institute Intramural Research Program ZIA EY000498-09.

Disclosure: **A.M. Allahdina**, None; **P.F. Stetson**, Carl Zeiss Meditec (E), P; **S. Vitale**, None; **W.T. Wong**, None; **E.Y. Chew**, None; **F.L. Ferris III**, None; **P.A. Sieving**, None; **C. Cukras**, None

References

1. Ben-Zvi I, Kivity S, Langevitz P, Shoenfeld Y. Hydroxychloroquine: from malaria to autoimmunity. *Clin Rev Allergy Immunol*. 2012;42:145–153.
2. Tehrani R, Ostrowski RA, Hariman R, Jay WM. Ocular toxicity of hydroxychloroquine. *Semin Ophthalmol*. 2008;23:201–209.
3. Yam JC, Kwok AK. Ocular toxicity of hydroxychloroquine. *Hong Kong Med J*. 2006;12:294–304.
4. Mititelu M, Wong BJ, Brenner M, Bryar PJ, Jampol LM, Fawzi AA. Progression of hydroxychloroquine toxic effects after drug therapy cessation: new evidence from multimodal imaging. *JAMA Ophthalmol*. 2013;131:1187–1197.
5. Marmor MF, Kellner U, Lai TY, et al. Revised recommendations on screening for chloroquine and hydroxychloroquine retinopathy. *Ophthalmology*. 2011;118:415–422.
6. Marmor MF, Kellner U, Lai TY, et al. Recommendations on screening for chloroquine and hydroxychloroquine retinopathy (2016 revision). *Ophthalmology*. 2016;123:1386–1394.
7. Browning DJ. Impact of the revised American Academy of Ophthalmology guidelines regarding hydroxychloroquine screening on actual practice. *Am J Ophthalmol*. 2013;155:418–428.e1.
8. Marmor MF. Efficient and effective screening for hydroxychloroquine toxicity. *Am J Ophthalmol*. 2013;155:413–414.
9. Chen E, Brown DM, Benz MS, et al. Spectral domain optical coherence tomography as an effective screening test for hydroxychloroquine retinopathy (the "flying saucer" sign). *Clin Ophthalmol*. 2010;4:1151–1158.
10. Kahn JB, Haberman ID, Reddy S. Spectral-domain optical coherence tomography as a screening technique for chloroquine and hydroxychloroquine retinal toxicity. *Ophthalmic Surg Lasers Imaging*. 2011;42:493–497.
11. Bernstein HN. Ocular safety of hydroxychloroquine. *Ann Ophthalmol*. 1991;23:292–296.
12. Lally DR, Heier JS, Baumal C, et al. Expanded spectral domain-OCT findings in the early detection of hydroxychloroquine retinopathy and changes following drug cessation. *Int J Retina Vitreous*. 2016;2:18.
13. Marmor MF. Comparison of screening procedures in hydroxychloroquine toxicity. *Arch Ophthalmol*. 2012;130:461–469.
14. Kellner S, Weinitz S, Kellner U. Spectral domain optical coherence tomography detects early stages of chloroquine retinopathy similar to multifocal electroretinography, fundus autofluorescence and near-infrared autofluorescence. *Br J Ophthalmol*. 2009;93:1444–1447.
15. de Sisternes L, Hu J, Rubin DL, Marmor MF. Localization of damage in progressive hydroxychloroquine retinopathy on and off the drug: inner versus outer retina, parafovea versus peripheral fovea. *Invest Ophthalmol Vis Sci*. 2015;56:3415–3426.
16. Cukras C, Huynh N, Vitale S, Wong WT, Ferris FL III, Sieving PA. Subjective and objective screening tests for hydroxychloroquine toxicity. *Ophthalmology*. 2015;122:356–366.
17. Stetson PF, Yehoshua Z, Garcia Filho CA, et al. OCT minimum intensity as a predictor of geographic atrophy enlargement. *Invest Ophthalmol Vis Sci*. 2014;55:792–800.
18. Hood DC, Bach M, Brigell M, et al. ISCEV standard for clinical multifocal electroretinography (mfERG) (2011 edition). *Doc Ophthalmol*. 2012;124:1–13.
19. Lyons JS, Severns ML. Detection of early hydroxychloroquine retinal toxicity enhanced by ring ratio analysis of multifocal electroretinography. *Am J Ophthalmol*. 2007;143:801–809.
20. Spaide RF, Curcio CA. Anatomical correlates to the bands seen in the outer retina by optical coherence tomography: literature review and model. *Retina*. 2011;31:1609–1619.
21. Browning DJ. *Hydroxychloroquine and Chloroquine Retinopathy*. Charlotte, NC: Springer; 2014:65–79.
22. Lujan BJ, Roorda A, Knighton RW, Carroll J. Revealing Henle's fiber layer using spectral domain optical coherence tomography. *Invest Ophthalmol Vis Sci*. 2011;52:1486–1492.
23. Napel S, Rubin GD, Jeffrey RB Jr. STS-MIP: a new reconstruction technique for CT of the chest. *J Comput Assist Tomogr*. 1993;17:832–838.
24. Neri E, Caramella D, Bartolozzi C, eds. *Image Processing in Radiology: Current Applications*. Berlin, Germany: Springer Verlag; 2008:55–66.
25. Isaac B. *Handbook of Medical Image Processing and Analysis*. 2nd ed. Burlington, MA: Elsevier Academic Press; 2009:10–17.
26. Niu S, de Sisternes L, Chen Q, Rubin DL, Leng T. Fully automated prediction of geographic atrophy growth using quantitative spectral-domain optical coherence tomography biomarkers. *Ophthalmology*. 2016;123:1737–1750.
27. Faraggi D, Simon R. A simulation study of cross-validation for selecting an optimal cutpoint in univariate survival analysis. *Stat Med*. 1996;15:2203–2213.
28. Perkins NJ, Schisterman EF. The inconsistency of "optimal" cutpoints obtained using two criteria based on the receiver operating characteristic curve. *Am J Epidemiol*. 2006;163:670–675.
29. Wolfe F, Marmor MF. Rates and predictors of hydroxychloroquine retinal toxicity in patients with rheumatoid arthritis and systemic lupus erythematosus. *Arthritis Care Res (Hoboken)*. 2010;62:775–784.
30. Marmor MF, Carr RE, Easterbrook M, et al. Recommendations on screening for chloroquine and hydroxychloroquine retinopathy: a report by the American Academy of Ophthalmology. *Ophthalmology*. 2002;109:1377–1382.
31. Altman DG, Lausen B, Sauerbrei W, Schumacher M. Dangers of using "optimal" cutpoints in the evaluation of prognostic factors. *J Natl Cancer Inst*. 1994;86:829–835.
32. Hilsenbeck SG, Clark GM, McGuire WL. Why do so many prognostic factors fail to pan out? *Breast Cancer Res Treat*. 1999;22:197–206.